AIAA Meeting Papers on Disc, July 1996
A9637206, N00014-95-1-0163, AIAA Paper 96-3075

Simulation of controlled injection of toxic waste for enhanced destruction in a compact incinerator

S. Arunajatesan
Georgia Inst. of Technology, Atlanta

S. Menon
Georgia Inst. of Technology, Atlanta

AIAA, ASME, SAE, and ASEE, Joint Propulsion Conference and Exhibit, 32nd, Lake Buena Vista, FL, July 1-3, 1996

Large Eddy Simulations (LES) of waste incineration in a dump combustor were performed. The results concerning the waste Destruction and Removal Efficiencies (DRE's) are presented and compared with experimental results. It is shown that significant increase in the DREs of the waste injected into the shear layer of the dump combustor can be obtained by forcing the inlet and fuel streams. The forcing of the inflow at the preferred mode causes an increase in the turbulence intensity levels close to the dump. This is shown to significantly enhance mixing of the fuel and air streams and advance the combustion zone upstream, thus causing an increase in waste destruction rates, (Author)

Simulation of Controlled Injection of Toxic Waste for Enhanced Destruction in a Compact Incinerator*

S. Arunajatesan† and S. Menon‡
School of Aerospace Engineering
Georgia Institute of Technology
Atlanta,GA 30332-0150

Abstract

Large Eddy Simulations (LES) of waste incineration in a dump combustor were performed. The results concerning the waste Destruction and Removal Efficiencies (DRE's) are presented and compared with experimental results. It is shown that significant increase in the DRE's of the waste injected into the shear layer of the dump combustor can be obtained by forcing the inlet and fuel streams. The forcing of the inflow at the preferred mode causes an increase in the turbulence intensity levels close to the dump. This is shown to significantly enhance mixing of the fuel and air streams and advance the combustion zone upstream, thus causing an increase in waste destruction rates.

1 Introduction

Incineration as a toxic waste disposal technique is an attractive alternative to other forms of waste disposal like landfills etc.. It provides a significant reduction in waste volume and allows for the recovery of energy in the form of heat. Also, many chemicals are rendered less toxic by raising them to higher oxidation states. However, current public opposition to transporting large amounts of waste to incineration sites has restricted the development of this methodology. In addition, current designs of these combustors do not allow for scaling up and down of these devices economically. Thus, there is a strong incentive to develop compact incinerators that are scalable and can consume large amounts of waste efficiently.

In this paper we present some results from a research effort to develop compact waste incinerators using dump combustors. The sudden expansion in a dump combustor causes the formation of a recirculation region and a shear layer behind the dump. A typical feature of the shear layer is the presence of large scale vortical structures. These structures grow by entraining mass into the shear layer. Hence, it is expected that the fuel/waste surrogate, when injected suitably, can be entrained into the shear layer causing efficient mixing and combustion.

Earlier studies on similar geometries have shown that the nature of the shear layer is strongly affected by the acoustic signature of the dump combustor. Wilson et al.[1] found that the acoustic modes in the combustor were controlled by the natural modes of the inlet duct. Further, they found the shear layer to be most responsive to forcing when the Strouhal number lay in the range 0.2-0.6. Similar results were also observed by Gutmark et al. [2] in free shear layers. They found that forcing the jet at its preferred mode and the coflowing fuel stream at higher harmonic of this mode caused an earlier transition to turbulence in the shear layer of the jet and thus, enhanced mixing and advanced the combustion region. In another paper, Logan et al. [3] studied the acoustic nature of the dump combustor. They found that three longitudinal modes exist in the dump combustor, a low frequency 'chugging' mode and two high frequency modes. Marchant et al. [4], in another related work found that the hydrodynamic modes of instability also play a dominant role in the dynamics of the combustor when the scale of operation was increased. Under conditions of strong acoustic output, the greatly increased growth rate of the vortices in the dump resulted in larger flame surface areas and hence, higher burning rates. Earlier, Zukoski and co-workers [5, 6] showed the presence of a strong coupling between the vortices shed at the dump and the acoustic nature of the dump combustors.

†Graduate Research Assistant,Student Member,AIAA

‡Associate Professor,Senior Member, AIAA

In the present work, using Large eddy Simulation (LES), this strong coupling between the shear layer dynamics and the dominant hydrodynamic and acoustic modes is used to enhance the consumption of waste surrogates injected into the shear layer behind the dump. A device that is currently being used for experimental demonstration [7] is numerically modelled in this study. Ethylene is used as the fuel and Benzene is used the toxic waste surrogate. Forced injection of the fuel/waste mixture is simulated identical to the method employed in the experimental study. The combustion efficiency of the forced fuel-air combustion is demonstrated by comparison with experimental results.

2 Governing Equations

In LES, only the length scales of the flow greater than the grid resolution are resolved while the unresolved scales are modelled. Hence, the governing equations for LES are obtained by filtering the equations of conservation of mass, momentum, energy and species. This is done by convolving the governing equations with a function of characteristic length scale equal to the grid spacing, Δ. In previous studies, various filter functions have been used. In this study, the box filter function is used which is well suited for finite volume schemes. For any arbitrary scalar f, the filtering operation and the filter function are defined as follows,

$$\tilde{f} = \int_D fG(\bar{r} - \bar{r}')dr' \tag{1}$$

$$G(\bar{r} - \bar{r}') = \frac{1}{\Delta}\begin{cases} \Delta & \text{if } |\bar{r} - \bar{r}'| < \Delta \\ 0 & \text{otherwise} \end{cases} \tag{2}$$

For axisymmetric geometries, the filtered form of the governing equations are written as follows,

$$\frac{\partial Q}{\partial t} + \frac{\partial F}{\partial x} + \frac{1}{y}\frac{\partial yG}{\partial y} = H \tag{3}$$

The vectors Q, F, G and H are given as follows,

$$Q = \begin{bmatrix} \bar{\rho} \\ \bar{\rho}\tilde{u} \\ \bar{\rho}\tilde{v} \\ \bar{\rho}\tilde{E} \\ \bar{\rho}\tilde{Y}_k \end{bmatrix} \tag{4}$$

$$F = \begin{bmatrix} \bar{\rho}\tilde{u} \\ \bar{\rho}\tilde{u}^2 + \bar{p} - \bar{\tau}_{xx} + {\tau_{xx}}^{sgs} \\ \bar{\rho}\tilde{u}\tilde{v} - \bar{\tau}_{xy} + {\tau_{xy}}^{sgs} \\ (\bar{\rho}\tilde{E} + \bar{p})\tilde{u} - \bar{\tau}_{xx}\tilde{u} - \bar{\tau}_{xy}\tilde{v} + \bar{q}_x + {H_x}^{sgs} + {\sigma_x}^{sgs} \\ \bar{\rho}\tilde{u}\tilde{Y}_k + \bar{\rho}\tilde{Y}_k\tilde{U}_k + {Y_{k,x}}^{sgs} \end{bmatrix} \tag{5}$$

$$G = \begin{bmatrix} \bar{\rho}\tilde{v} \\ \bar{\rho}\tilde{u}\tilde{v} - \bar{\tau}_{xy} + {\tau_{xy}}^{sgs} \\ \bar{\rho}\tilde{v}^2 + \bar{p} - \bar{\tau}_{yy} {\tau_{yy}}^{sgs} \\ (\bar{\rho}\tilde{E} + \bar{p})\tilde{v} - \bar{\tau}_{xy}\tilde{u} - \bar{\tau}_{yy}\tilde{v} + \bar{q}_y + {H_y}^{sgs} - {\sigma_y}^{sgs} \\ \bar{\rho}\tilde{v}\tilde{Y}_k + \bar{\rho}\tilde{Y}_k\tilde{V}_k + {Y_{k,y}}^{sgs} \end{bmatrix} \tag{6}$$

$$H = \begin{bmatrix} 0 \\ 0 \\ \bar{p} - \bar{\tau}_{\theta\theta} \\ 0 \\ \bar{\omega}_k \end{bmatrix} \tag{7}$$

where, $\bar{\rho}$ is the density, $\tilde{u}$ and $\tilde{v}$ are the axial and radial velocity components respectively, $\bar{p}$ is the pressure, $\bar{\tau}_{xx}$, $\bar{\tau}_{xy}$,$\bar{\tau}_{yy}$ and $\bar{\tau}_{\theta\theta}$ are the components of the stress tensor. $\tilde{E}$ is the total energy per unit mass, $\tilde{Y}_k$ is the mass fraction of the k^{th} species, $\bar{\omega}_k$ is the production rate of the k^{th} species due to chemical reactions and $\bar{q}_x$ and $\bar{q}_y$ are the components of the heat flux vector. $\tilde{U}_k$ and $\tilde{V}_k$ are the axial and radial components of the diffusion velocity of the k^{th} species. $\tilde{E}$, the total energy is given by,

$$\tilde{E} = \tilde{e} + \frac{(\tilde{u}^2 + \tilde{v}^2)}{2} \tag{8}$$

where, $\tilde{e}$ is the internal energy. $\tilde{e}$ is written as,

$$\tilde{e} = \tilde{h} - \frac{\bar{p}}{\bar{\rho}} \tag{9}$$

where, $\tilde{h} = \sum_{k=1}^{N} \tilde{Y}_k\tilde{h}_k$ is the specific enthalpy of the mixture. Here, $\tilde{h}_k$, is the specific enthalpy of the k^{th} species. All the species are assumed to be calorically perfect, giving the following expression for $\tilde{h}_k$,

$$\tilde{h_k} = {h^o}_{f,k} + C_{p,k}(\tilde{T} - T^o) \tag{10}$$

where, ${h^o}_{f,k}$ is the heat of formation at the reference temperature T^o. T^o is chosen as 298K in this study.

The stress tensor is expressed in terms of the velocity gradients as follows, (in tensor notation)

$$\bar{\tau}_{ij} = \bar{\mu}\left(\frac{\partial \tilde{u}_i}{\partial x_j} + \frac{\partial \tilde{u}_i}{\partial x_j}\right) - \frac{2}{3}\bar{\mu}\delta_{ij}\frac{\partial \tilde{u}_k}{\partial x_k} \tag{11}$$

Sutherland's law is used to calculate $\bar{\mu}$ as a function of temperature. The heat flux vector is expressed in terms of the temperature gradients and the species diffusion velocities as

$$\bar{q}_x = -\lambda\frac{\partial \tilde{T}}{\partial x} + \sum_{k=1}^{N} \bar{\rho}\tilde{Y}_k\tilde{U}_k\tilde{h}_k \tag{12}$$

$$\bar{q}_y = -\lambda\frac{\partial \tilde{T}}{\partial x} + \sum_{k=1}^{N} \bar{\rho}\tilde{Y}_k\tilde{V}_k\tilde{h}_k \tag{13}$$

where, λ is the thermal conductivity.

The species are assumed to follow Fickian diffusion. Thus,

$$\bar{\rho}\tilde{Y}_k\tilde{U}_k = -\bar{\rho}D_k\frac{\partial\tilde{Y}_k}{\partial x} \tag{14}$$

$$\bar{\rho}\tilde{Y}_k\tilde{V}_k = -\bar{\rho}D_k\frac{\partial\tilde{Y}_k}{\partial y} \tag{15}$$

where D_k is the diffusivity of the k_{th} species. The diffusivities for all the species are assumed to be equal in this work. Further, the Lewis number is assumed to be equal to unity for all the species.

The production rate term in the species equations is calculated from the chemical reaction mechanism. Since the time scales of the chemical reactions are typically several orders of magnitude smaller than those of the convection and diffusion processes, the source term restricts the time step size that can be used in the simulations. This restriction can be very severe and can drastically affect the computational feasibility of a simulation. However, by specially treating this term, this restriction can be overcome to a large extent. In this work, we adopt a decoupled technique based on the work by Calhoon et al. [8] to calculate the source term at each time step. The details of this method are given later.

The superscript *sgs* in the above equations represent the additional terms arising due to the filtering operation performed on the governing equations. These additional terms are given as follows, (in tensor notation)

$${\tau_{ij}}^{sgs} = \bar{\rho}(\widetilde{u_iu_j} - \tilde{u}_i\tilde{u}_j) \tag{16}$$

$${H_i}^{sgs} = \bar{\rho}(\widetilde{Eu_i} - \tilde{E}\tilde{u}_i) + (\widetilde{pu_i} - \bar{p}\tilde{u}_i) \tag{17}$$

$${\sigma_i}^{sgs} = (\tau_{ij}\bar{u}_j - \bar{\tau}_{ij}\tilde{u}_j) \tag{18}$$

These terms are not known in terms of the resolved quantities and hence need to be modeled. Some of the well known models for these terms include the Smagorinsky model [9], or its compressible extension proposed by Erlebacher [10]. Both these models rely the eddy viscosity hypothesis and use dimensional analysis to arrive at ad-hoc expressions for the eddy viscosity. The constants appearing in these models need to be specified apriori and are computed from direct simulations of simple flows. In more complex flows like dump combustors or backward facing steps, the use of these constants derived from simple flows is questionable. Another fast developing approach to modeling these terms is the dynamic evaluation of these constants [11]. In this approach, the constants are evaluated in terms of the resolved variables as a function of space and time. This method requires the assumption of scale similarity between the resolved scales and a test filter level. Although these methods yield significantly better results than the constant coefficient methods, they are very expensive to implement and still rely on the eddy viscosity hypothesis.

In the present work, we have chosen to neglect these terms. Earlier work on solid fuel combustion chambers [12] and mixing layers [13] have shown that neglecting these unresolved terms does not affect the results significantly in two dimensional and axisymmetric simulations. However, in the present work, in the reacting flow simulations, the molecular viscosity is assumed to remain constant at the reference value. This may be thought of as a zeroth order model for the unresolved terms. This method has been shown to yield good results for flows in ramjets [14] for reacting and non-reacting flows. Also, the flows of interest here, namely, dump combustor flows, are dominated by the large scale structure dynamics. Since these scales are fully resolved, it is expected that the simulation should be capable of capturing the large scale effects accurately using this simplified model.This is indeed seen to be the case as seen from the validation and reacting flow results which compare very well with experimental results.

3 Numerical Implementation

The governing equations described in the previous section are solved numerically using the fourth order extension of the MacCormack Scheme proposed by Turkel et al. [15]. The unsteady equations are marched in time using the second order Runge-Kutta scheme. At the boundaries, the accuracy of the scheme is lowered to second order. The boundary conditions at the inflow and outflow are handled using the characteristic boundary conditions of Poinsot and Lele [16]. No slip and adiabatic conditions are imposed at the walls and symmetry conditions are imposed on the centreline.

This code was implemented on multiple processors on parallel machines like the Intel-Paragon, the IBM-SP2 and the Cray-T3D. This was accomplished by the decomposing the computational domain (shown in Fig. 1a) into smaller domains(Fig. 1b) and solving each one of the smaller domains on one processor. The computational grid is initially generated off line using a single processor grid generator. The appropriate portion of the grid is then read in by each processor such that the load (mea-

sured in terms of the number of computational nodes per processor) is approximately equal on each processor. At each step, each processor requires information about the computational nodes adjoining its boundaries. This is handled by maintaining a small overlap of three computational nodes between adjacent processors. The values of flow field variables at these overlap nodes is updated every step by explicit message passing. This is done using message passing libraries of Message Passing Interface (MPI) [17]. This library contains various communication routines that can be used to exchange information between the processors. It also has the advantage that it is completely portable between machines. Thus, only one code needs to be maintained and can be used on any machine as required. Since the domain sizes are different in the inlet and combustor regions, different processor distributions are used in the two regions. Although a balance in the load distribution is still maintained, this difference in the processor distributions requires that the corner the inter-processor communication be handled specially. A generic algorithm developed by Menon and Weeratunga [18] is used to ensure correct communication between the processors on either side of the step.

Results from some timing tests conducted on three machines, namely, Intel-Paragon, IBM-SP2 and Cray-T3D, are presented in Figs. 2a, 2b and 2c, respectively. The geometry used was the same as the one used in our incineration studies. The grid used in these tests consisted of 288 points in the axial direction and 64 points in the transverse direction. The three figures show the performance of the three machines as the problem complexity is increased. The same problems were run on 16, 32, 64 and 128 processors to study the scale up achieved. In an implementation of the kind used here, although increasing the number of processors reduces the load on each processor in terms of the number of computational nodes it has to handle, the increase in the number of processors causes an increase in the amount of message passing to be handled for the overlap nodes. These two factors are in conflict and it is to be expected that the overheads due to the increased communication will surpass the gains due to the reduced number of computational nodes per processor at some point. This is clearly visible in the data for the SP-2 machine. For this machine the optimal number of processors for the grid size used seems to lie around 32 or a grid of 32 x 16 points per processor. For the other two machines, however,this limit is not reached within 128 processors. Due to limitations in the available machine sizes larger decompositions could not be tested. But, it is seen that the gain in CPU times shows diminishing returns as the number of processors is increased for the chosen grid resolution. A more detailed study of the timings and other issues like I/O overheads etc. is presented elsewhere [19] and the reader is referred to that paper for more details. A full simulation for a typical case presented here took approximately 48 hours of CPU time on a 64 processor Intel-Paragon.

4 Reaction Mechanism

For the reacting flow simulations, the fuel used was Ethylene and the waste surrogate was Benzene. The reaction mechanism for both these compounds have been studied extensively [20, 21, 22, 23]. These mechanisms are extremely complex and involve 277 reactions among 48 species for ethylene and 110 reactions among 35 species for benzene. Even on the Massively Parallel systems, it would be computationally infeasible to use these mechanisms in their full form. Hence, a simplified mechanism based on this full mechanism has been developed for this study. The main criteria used to develop these mechanisms were the accurate prediction of the temperature profiles and the profiles of the major product species.

The methodology used to obtain the reduced mechanism was originally suggested by Singh and Jachimowski [24]. In their method, the initial breakdown of ethylene and benzene is assumed to occur according to the reactions,

$$C_2H_4 + 3O_2 \rightleftharpoons 2CO_2 + 2H_2O \qquad (19)$$

$$C_6H_6 + 7.5O_2 \rightleftharpoons 6CO_2 + 3H_2O \qquad (20)$$

The rest of the mechanism is made up of reactions that describe the oxidation of CO and H_2.

Another important issue today is the emission of pollutants from systems such as that which is being studied here. Recent Governmental regulations have led to studies to reduce emission of chemicals such as the oxides of nitrogen (NO_x) and carbon-monoxide from these combustors. In order to be able to study these issues, we have also included a simplified mechanism for the formation of NO. This mechanism was originally proposed by Chen and Kollmann [25] . It is a simplified version of the well known three step Zeldovich mechanism for NO formation in reacting systems. Using a steady state assumption for the N atom and that $[NO]/[NO]_{equil.} \ll 1$ they reduced the three step Zeldovich mechanism to a one step global reaction given by,

$$N_2 + O_2 \rightleftharpoons 2NO \qquad (21)$$

The NO formation rate is approximated by

$$\dot{\omega}_{NO} = 2k_f[N_2][O]W_{NO} \tag{22}$$

The reaction rate coefficients of all the reactions are given in the form

$$\omega = AT^n exp\left(\frac{E_a}{RT}\right) \tag{23}$$

The coefficients A, n and E_a are given in Table 1.

Table 1. Reaction Mechanism Coefficients[1]

Reaction	A	n	E_a
$C_2H_4 + 3O_2 \rightleftharpoons 2CO_2 + 2H_2O$	2.2e11	0.0	1.5558e8
$C_6H_6 + 3O_2 \rightleftharpoons 6CO + 3H_2$	1.8e8	0.0	1.4859e8
$CO + O \rightleftharpoons CO_2 + M$	5.3e1	0.0	-1.9004e7
$CO + OH \rightleftharpoons CO_2 + H$	4.4	1.5	-3.0975e6
$H_2 + O_2 \rightleftharpoons OH + OH$	1.7e7	0.0	2.0092e8
$H + O_2 \rightleftharpoons OH + O$	2.6e8	0.0	7.0322e7
$OH + H_2 \rightleftharpoons H_2O + H$	2.2e7	0.0	2.1557e7
$O + H_2 \rightleftharpoons OH + H$	1.8e4	0.0	3.7254e7
$OH + OH \rightleftharpoons H_2O + O$	6.3e7	0.0	4.5626e6
$H + H \rightleftharpoons H_2 + M$	6.4e5	-1.0	0.0
$H + OH \rightleftharpoons H_2O + M$	2.2e10	-2.0	0.0
$N_2 + O_2 \rightleftharpoons 2NO$	1.82e8	0.0	1.6061e8

The coefficients for the reactions describing the oxidation of CO and $H2$ are obtained from the detailed mechanism [20]. The coefficients for the initial breakdown reactions are chosen to give the best agreement with the detailed mechanism for the temperature and major product species profiles.

The proposed mechanism was tested against the detailed mechanism for the classical point problem . The reactions were assumed to occur at constant pressure. Three different equivalence ratios, $\phi = 0.5$, $\phi = 1.0$ and $\phi = 2.0$ were tested. The results of the point problem simulations are shown in Figs. 3a-3c alongwith the results from the detailed mechanism applied to the same problems. It is seen that the agreement between the predictions of the proposed mechanism and those of the detailed mechainsm is very good for all the cases considered. The CO_2 profiles are slightly overpredicted by the proposed mechanism for the rich case. However, since the equivalence ratios in the dump combustor simulations are very lean, this is not expected to affect the results greatly.

[1]Units are in seconds, Kg., m^3, J and degrees Kelvin. Third Body efficiencies for all thermolecular reactions are 2.5 for $M = H_2$,16.0 for $M = H_2O$ and 1.0 for all other M

5 Source Term Computation

The computation of the source term was done using a decoupled technique based on the work by Calhoon et al. [8].In this method, the source term computation at each point at each time step is considered as a point problem at constant pressure. This point problem is then solved to obtain the source term for that time step.This is done by solving the following equations,

$$\frac{dY_k}{dt} = \frac{\dot{\omega}_k}{\rho} \tag{24}$$

$$\frac{dT}{dt} = \frac{1}{\rho C_p}\sum_{k=1}^{N}\dot{\omega}_k h_k \tag{25}$$

The source term for the LES solver is then computed by simply integrating the source term from the point problem solver. The point problem, however, needs to be calculated at the time scales demanded by the chemistry. This is done using an ordinary differential equation solver from the NETLIB package.

6 Code Validation

In order to establish the capability of the simulation code, we conducted a simple validation study. Flow past a backward facing step, which is very similar to the dump combustor was chosen for our study. The geometry studied by Moin and Le in their DNS simulations [26] was chosen for this purpose. The experimental data of Jovic and Driver presented in that paper was also used for comparison. This experimental data appears not yet to have been published elsewhere. The results presented here are from a two dimensional simulation whereas the DNS results used for comparison are from a three dimensional simulation. Since the backward facing step flow is dominated by the large two-dimensional structures formed at the step, a two dimensional simulation is expected to capture the effects of these structures. The resolution used in these studies was 256x96 and the Reynolds number based on the step height was 5100 and the mean inlet velocity was $15m/s$. The geometry parameters are identical to those used by Moin and Le in their study. In order to simulate realistic inflow turbulence, random velocity fluctuations were superimposed on the mean flow field at the inlet. The rms value of the fluctuation was maintained at 15 percent.

Comparison of the mean flow velocity profiles is presented in Fig. 4a. The results from the present simulations agree very well with those from

the DNS and the experiments. The observed reattachment length was $5.9h$ where h is the step height. The DNS results yielded a value of $6.1h$ as against the experimental value of $6.2h$. Fig. 4b shows the comparison of the predicted wall pressure coefficient against the DNS and experimental data. The results do not agree very well in the strongly recirculating regions. In these regions, the flow field is highly three dimensional and a two dimensional simulation may not be able to capture the three dimensional effects fully. However, the large scale dynamics of the flow are captured accurately as is seen from the velocity profiles.This is particularly relevant to our study since we are interested in the large scale features of the flow. The close agreement between the predicted reattachment length and the DNS value seem to indicate that the difference in the pressure profile is a local effect.

Figs. 4c-4e show the comparison of the turbulence intensity profiles. The reasonably good agreement in this data seems to indicate that the turbulent characteristics of the large scale flow field are accurately captured in the present simulations. This is very crucial, because, in the dump combustor simulations, the accurate prediction of mixing of the fuel/waste stream and the inflow air stream is critical to accurate predictions of the waste DRE's.

7 Results and Discussion

In this work, two different configurations were studied. The first one was a simple sudden expansion pipe. In this configuration, the inlet pipe of diameter D is suddenly expanded to a diameter $4.68D$. The expansion ratio and the lengths are chosen to correspond to those of a combustor being simultaneously studied experimentally at Naval Weapons Research Center, Chinalake. The second geometry is the one shown in Fig.1 . It has the same expansion ratio and the lengths as the first configuration except that it has an area blockage lip at the tail end of the combustor identical to the one being studied experimentally at NWRC, Chinalake.

This area blockage lip plays an important role in determining the dynamics of the combustor flow field. The blockage lip is an acoustic reflector and its presence amplifies the acoustic oscillations in the combustor. Fig. 5a and 5b show the time trace of pressure in the combustor close to the exit plane with and without the area blockage lip. It is seen that the amplitude of the pressure oscillations in the dump combustor is amplified nearly 10 times in the presence of the area blockage lip. However, it must be noted that the frequency content of the pressure signal is not significantly altered. The Fourier transform of the pressure signals for both these cases are shown in Figs. 5c and 5d . The most dominant mode in both the cases has a frequency of 200Hz. In the geometry with the lip, the amplitude of the higher harmonics of the pressure signal are also amplified. This lip acts as a reflection surface for the backward traveling acoustic waves [27]. This results in a standing wave pattern being setup in the combustor causing a phase-locking phenomenon to occur between the acoustic waves and the vortex shedding at the step. However, having a large area blockage lip will accelerate the flow at the exit causing a suction which will reduce the residence times of the waste surrogates injected into the dump. In our simulations the length of the lip chosen to agree with the experimental configuration and the resulting area blockage was 50 percent. All the results presented here are from the simulation of the dump combustor with the area blockage lip.

Three different cases were studied on this configuration. The first one was a simple unforced flow, in which air at room temperature enters through the inlet duct and a mixture of fuel and waste is injected into the shear layer at the dump plane. In the second case, the inflow was forced at a frequency equal to that of the most dominant mode of the pressure signal in the combustor. In the third case, the fuel-waste mixture was also forced at the same frequency as the inlet.

In both cases, the amplitude of forcing was maintained at 15 percent, in agreement with the experimental configuration. The Strouhal number of this mode based on the inlet diameter and the inlet velocity is 0.498. Jets are known to be most responsive to excitation when the Strouhal number lies in the range 0.2-0.6 [28, 2]. Thus it is expected that forcing at this frequency is likely to have a very large impact on the dynamics of the flow in the combustor.

The fuel was injected into the shear layer layer at an angle of 15 degrees to the horizontal. The boundary conditions used were similar to those at the inlet and were based on the work of Poinsot and Lele [16]. An parabolic injection profile was used for the velocities and 16 points were used to resolve the injection port. The injection port was an annular ring of width 1.2mm located just above the dump plane. The mass flow rate of the mainstream air flow was $28gms/sec$ and the mass flow rate of the fuel-waste mixture was $1.06gms/sec$. Thus, clearly, the system is very fuel lean compared to the stoichiometric fuel mass flow rate of $5.88gms/s$. The

Reynolds number of the cold flow based on the step height was 7500. A constant stream of entrainment air flow was maintained at a rate of $8.1 gms/s$ from the outer wall of the combustor close to the dump plane to enable complete entrainment of the injected fuel-waste mixture into the shear layer. In all the cases the combustion was initiated by forced reaction at a few grid points. This transient was allowed to wash out before any data acquisition was done. The hot products in the recirculation zone then sustains the combustion for the rest of the simulation.

As in most combustion problems, the OH radical concentration was used as an indicator of the reaction zone. The OH concentration maps from the present simulations are shown in Fig. 6. Only one half of the symmetric flame is shown here. In the first frame (no forcing) (Fig. 6a), there is a clear stand off distance between the dump and the flame tip. There is practically no combustion in the region between the dump and the first roll-up. This is due to poor mixing of the fuel and air streams and due to the high strain rates in this region. However, at the periphery of the first roll-up, the reaction rate is seen to pick up due to better mixing of the fuel and fairly large OH concentrations are observed in the roll-up. However, the absence of any mixing in the initial part of the shear layer delays combustion and hence, waste consumption. In the cases where the inlet stream and the fuel stream are forced (Fig. 6b), the combustion region is seen to move upstream towards the dump plane. The forcing of the inflow stream (in this case, at the preferred mode) causes an increase in the turbulence levels close to the dump region. This enhances the mixing of the fuel and air streams and results in the upstream advancement of the combustion zone. Forcing the fuel stream also seems to amplify this effect causing a further increase in the turbulence levels close to the dump plane. The shear layer is seen to grow faster, causing better entrainment and mixing of the injected fuel and waste.

These results are summarized quantitatively in Fig. 7. Here, the radially integrated OH concentration at each axial location across the flame width is shown. The data is normalized by the OH concentration in the unforced case at $X/D = 3.0$. It is seen clearly that, in the unforced case, the OH concentration levels are very low in the region $X/D < 2.0$ and it suddenly shoots up in the periphery of the first roll-up. In contrast to this, for the forced cases, the OH concentration increases steadily right from the dump plane. The large OH production in the initial region indicates a very rapid consumption of the fuel and waste surrogate in this region. This high consumption, in fact, causes a slight decrease in the OH concentration in the core of the first roll-up. Similar results were also observed in forced free shear layers by Gutmark et al. [2]. It should be noted that the combustion zone for the third case, where the fuel and waste are also forced is even closer to the dump plane than the other two cases. This fact is also reflected in the integrated OH concentration profiles.

Contour maps of vorticity in the vicinity of the dump plane are shown in Fig. 8. It is seen that, in the unforced case(Fig. 8a), there are hardly any structures between the first roll-up and the dump plane. However, when the inlet is forced (Fig. 8b), this region of high strain rates is seen to break down into smaller structures. When both the inlet and the fuel streams are forced (Fig. 8c), this region is seen to be full of small counter-rotating vortices indicated by the positive and negative signs in the figures. These vortices increase the turbulent transport in this initial region, increasing the cross-fluxes of the fuel and air streams. This results in better mixing of the fuel and air streams, bringing the combustion zone closer to the dump plane as discussed earlier.

Fig. 9a shows the turbulence intensity levels close to dump along the shear layer center-line for the three cases. Again, it is seen that the forcing causes an increase in the turbulence intensity in the initial region of the shear layer. The growth rates of the shear layer for the three cases are shown in Fig. 9b. It is seen that although the growth rate of the shear layer downstream of the dump plane is not greatly affected by the forcing, in the region close to the dump plane, the shear layer for the forced cases is much thicker. This enhanced thickness is due to the presence of a large number of small counter rotating vortices which aid in the transport of the fuel and air into the mixing zones. This greater mixing is seen to cause the advancement in the combustion zone observed in the OH concentration maps discussed earlier.

Fig. 10 shows the destruction and removal efficiencies for Benzene for the three cases. It is seen that for the forced cases, there is a significant increase in the destruction rates when compared to the unforced cases. The data shown here is obtained by radially integrating the Benzene concentration at each axial location. The DRE's are expressd in terms of the number of nines which is computed as follows,

$$\#of9's = -log_{10}(1.0 - \frac{\%consumption}{100}) \quad (26)$$

Hence, a consummtion of 99.99% yields a DRE of 4. It is seen that by forcing the inflow and the fuel streams, the destruction rates can be nearly doubled. It is also seen that the computational results obtained from these simulations agree fairly well with experimental measurements made on the same setup. The slight overprediction in the DRE levels is an artifact of the chemical reaction mechanism used. However, all the trends are captured correctly. The hump in all the three curves around X/D of 2.0 is due to the presence of the large scale roll up at that location. In the periphery of this roll-up, increased reaction rates occur due to better mixing of the fuel and air streams, thus causing a slight increase in the DRE's.

8 Conclusion

Numerical simulations of waste incineration in a dump combustor were performed to study the effect of forcing on the waste consumption rates. Forcing the inlet stream at the preferred mode of the incoming jet causes an increase in the turbulence levels in the regions close to the dump plane. This is accompanied by an increase in the growth rate of the shear layer in this near field region. The increased turbulence in the near field causes an enhancement in the fuel-air mixing rates close to the dump, resulting in an upstream advancement of the combustion zone. Forcing the fuel and waste stream aids this process, further advancing the combustion zone. This advancement in the combustion zone results in increased consumption rates of the injected waste.

Acknowledgments

This work was supported by Office of Naval Research/SERDP Program under grant No. N00014-95-1-0163. The simulations were performed on the DOD high performance computer systems at Wright Patterson AFB (Intel-Paragon), Eglin AFB (Cray-T3D) and the Maui high performance computing center (IBM-SP2). These contributions are gratefully acknowledged.

References

[1] Wilson, K.J., Gutmark, E., Schadow, K.C., Smith, R.A., Feedback Control of a Dump Combustor with Fuel Modulation, *Journal of Propulsion and Power*, Vol. 11, No. 2, March-April 1995.

[2] Gutmark, E., Parr, T.P., Hanson-Parr, D.M., Schadow, K.C., On the Role of Large and Small-Scale Structures in Combustion Control, *Combustion Science and Technology*, Vol. 66, pp 107-126, 1989.

[3] Logan, P., Lee, J.W., Lee, L.M., Karagozian, A.R., Acoustics of a Low-Speed Combustor, *Combustion and Flame* Vol. 84, pp 93-109, 1991.

[4] Marchant, R., Hepler, W., Smith, O.I., Willis, J., Cadou, C., Logan, P., Karagozian, A.R., Development of a Two-Dimensional Dump Combustor for the Incineration of Hazardous Wastes, *Combustion Science and Technology*, Vol. 82, pp 1-12, 1992.

[5] Smith, D.A., Zukoski, E.E., Combustion Instability Sustained by Unsteady Vortex Combustion, Twenty first Joint Propulsion Conference, Monterey,CA, Paper 1248, 1985.

[6] Sterling, J.D., and Zukoski, E.E. Longitudinal Mode Combustion Instabilities in a Dump Combustor, AIAA-87-0220, 1987.

[7] Parr, T.P., *Private Communication*

[8] Calhoon, W.H., Menon, S., Goldin, G., Comparison of Reduced and Full Chemical Mechanisms for Nonpremixed Turbulent H_2-Air Jet Flames *Combustion Science Technology*, Vol. 104, pp 115-141, 1995.

[9] Smagorinsky, J., General Circulation Experiments with the Primitive Equations, *Monthly Weather Review*, Vol. 91, No. 3, pp 99-164, 1963.

[10] Erlebacher, G., Hussaini, M.Y., Speziale, C.G., Zang, T.A., Toward the Large-Eddy Simulation of Compressible Turbulent Flows, ICASE 87-20, 1987.

[11] Menon, S., Kim, W.-W., High Reynolds Number Flow Simulations Using the Localized Dynamic Subgrid-Scale Model, AIAA-96-0425, 1996.

[12] Liou, T.M., Lien, W.Y., Hwang, P.W., Large-Eddy Simulations of Turbulent Reacting Flows in a Chamber with Gaseous Ethylene Injecting through the Porous Wall, *Combustion and Flame* Vol. 99, pp 591-600, 1994.

[13] Schwer, D.A., Tsuei, H.-H., Merckle, C.L., Computation and Validation of Spatially Developing Reacting Mixing Layers, AIAA-95-0261, 1995.

[14] Menon, S., Jou, W.-H., Large-Eddy Simulation of Combustion Instability in an Axisymmetric Ramjet Combustor, *Combustion Science and Technology*, Vol. 75, pp 53-72, 1991.

[15] Bayliss, A.,Parikh, P.,Maestrello, L.,Turkel, E., A Fourth-Order Scheme for the Unsteady Compressible Navier-Stokes Equations, NASA-CR-177994, 1985.

[16] Poinsot, T.J., and Lele, S.K., Boundary Conditions for Direct Simulations of Compressible Viscous Flows, *Journal of Computational Physics*, Vol. 101, pp104-129, 1992.

[17] MPI user guide

[18] Weeratunga, S., Menon, S., Parallel Computations of Unsteady Combustion in a Ramjet Engine, AIAA-93-1914, 1993.

[19] Menon, S., Parallel Simulations of Unsteady Turbulent Flames, Proceedings of EUROSIM Int. Conference on HPCN Challenges in Telecomp and Telecom, 1996.

[20] Dagaut, P., Cathonnet, M., Boettner, J.C., Gaillard, F., Kinetic Modeling of Ethylene Oxidation, *Combustion and Flame*, Vol. 71, pp 295-312, 1988.

[21] Dagaut,P., Cathonnet, M., Boettner, J.C., Experimental Study and Kinetic Modeling of Propene Oxidation in a Jet Stirred Flow Reactor, *Journal of Physical Chemistry*, Vol. 92 No. 3 pp 661-671, 1988.

[22] Bittker, D.A., Detailed Mechanism of Benzene Oxidation, NASA-TM-100202

[23] Lindstedt, R.P., Skevis, G., Detailed Modeling of Premixed Benzene Flames, *Combustion and Flame* Vol. 99, pp 551-561, 1994.

[24] Singh, D.J., and Jachimowski, C.J., Quasigloabal Reaction Model for Ethylene Combustion, *AIAA Journal* Vol. 32 No.1, pp 213-216, 1994.

[25] Chen, J.-Y., Kollmann, W., PDF Modeling and Analysis of Thermal NO Formation in Turbulent Nonpremixed Hydrogen-Air Jet Flames, *Combustion and Flame*, Vol. 88, pp 397-412, 1992.

[26] Le, H., Moin, P., Direct Numerical Simulation of Turbulent Flow over a Backward-Facing Step, CTR Annual Research Briefs, pp 161-173, 1992.

[27] Jou, W.-H., Menon, S., Modes of Oscillation in a Nonreacting Ramjet Combustor Flow, *Journal of Propulsion and Power*, Vol. 6 No. 5, pp 535-543, 1990.

[28] Gutmark, E., Ho, C.M., Preferred Modes and Spreading Rates of Jets, *Physics of Fluids* Vol. 26, No. 10, pp 2932-2938, 1983.

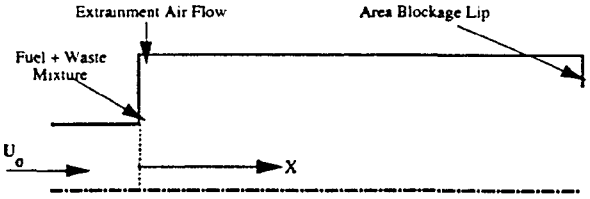

Fig.1a. Schematic of Dump Combustor Geometry used.

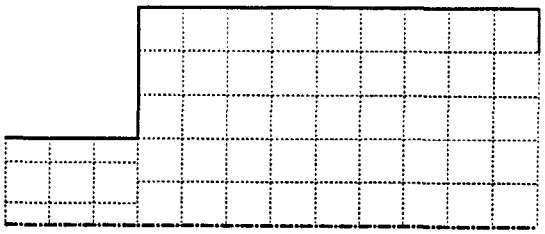

Fig.1b. Schematic representation of the Domain Decomposition for Parallel implementation.

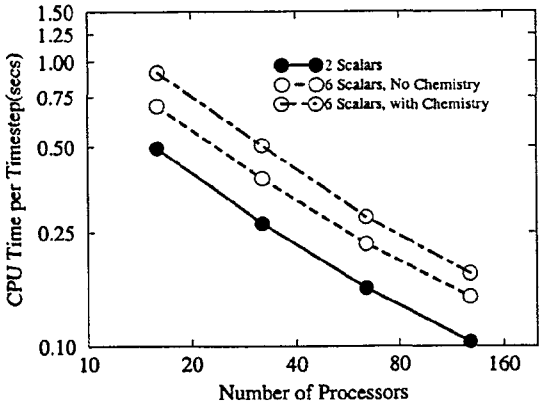

Fig.2a. Timing results for the Intel–Paragon.

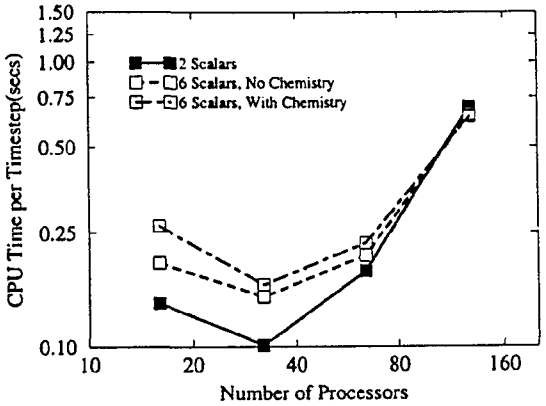

Fig.2b. Timing results for the IBM–SP2

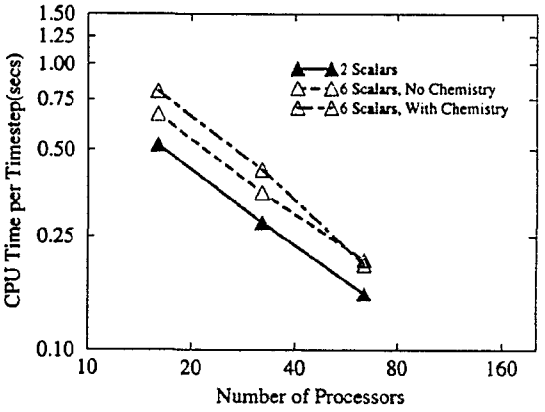

Fig.2c. Timing results for the Cray–T3D

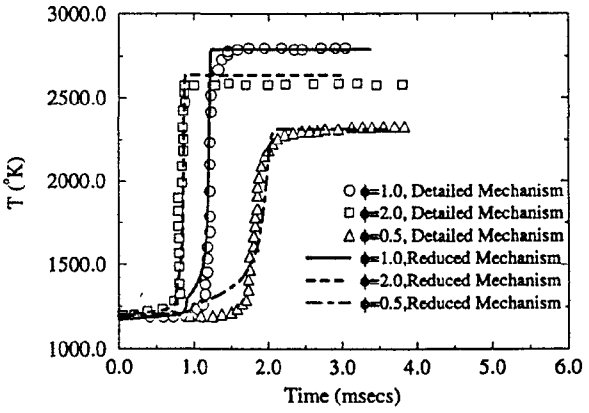

Fig.3a. Comparison of Temperature profiles predicted using the reduced and detailed reaction mechanisms.

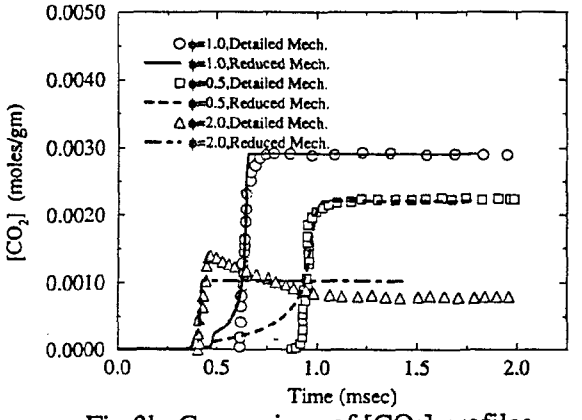

Fig.3b. Comparison of [CO_2] profiles predicted using the reduced and detailed reaction mechanisms.

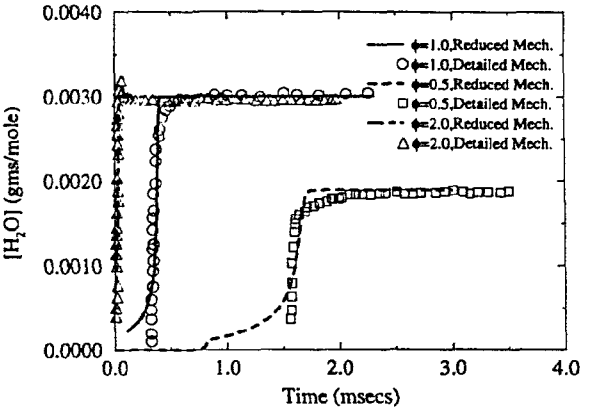

Fig.3c. Comparison of [H_2O] profiles predicted using the reduced and detailed reaction mechanisms.

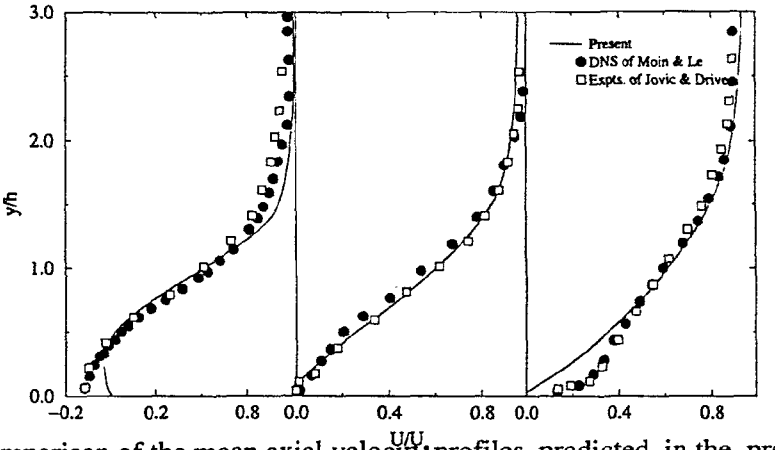

Fig. 4a. Comparison of the mean axial velocity profiles predicted in the present simulations against DNS of Moin and Le and experiments of Jovic and Driver. The profiles are shown at X/H = 4.0, X/H = 6.0 and X/H = 10.0.

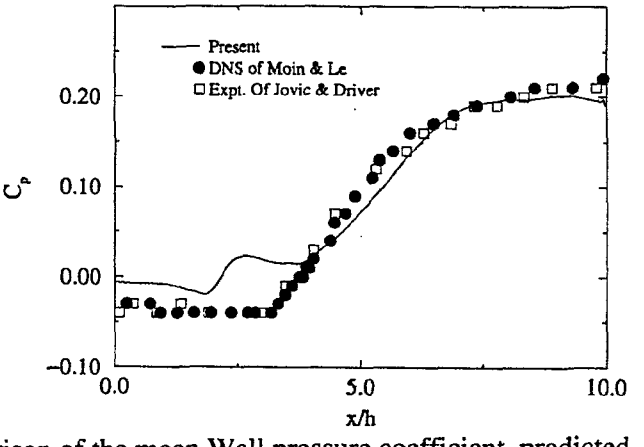

Fig. 4b. Comparison of the mean Wall pressure coefficient predicted in the present simulations against DNS of Moin and Le and experiments of Jovic and Driver

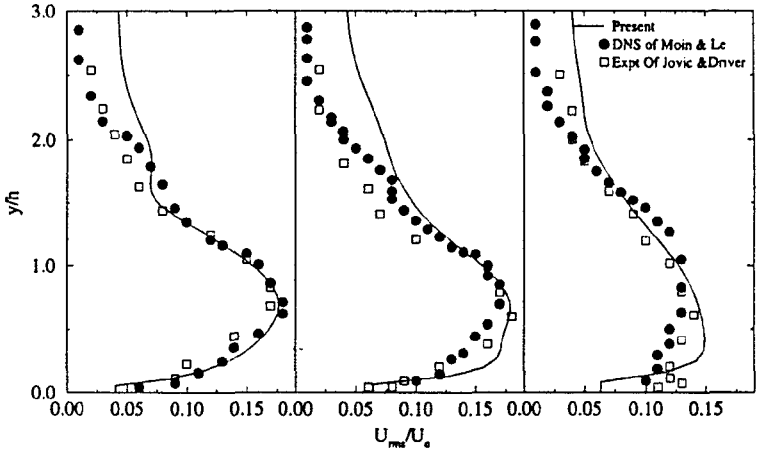

Fig. 4c. Comparison of the axial turbulence intensity profiles predicted in the present simulations against DNS of Moin and Le and experiments of Jovic and Driver. The profiles are shown at X/H = 4.0. X/H = 6.0 and X/H = 10.0.

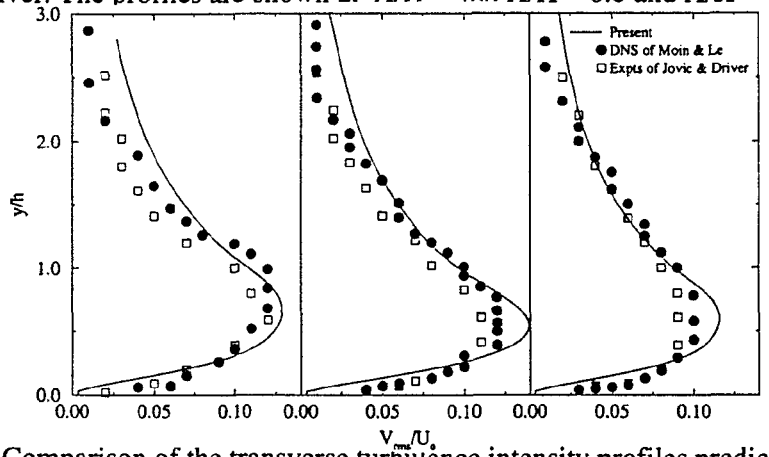

Fig. 4d. Comparison of the transverse turbulence intensity profiles predicted in the present simulations against DNS of Moin and Le and experiments of Jovic and Driver. The profiles are shown at X/H = 4.0, X/H = 6.0 and X/H = 10.0.

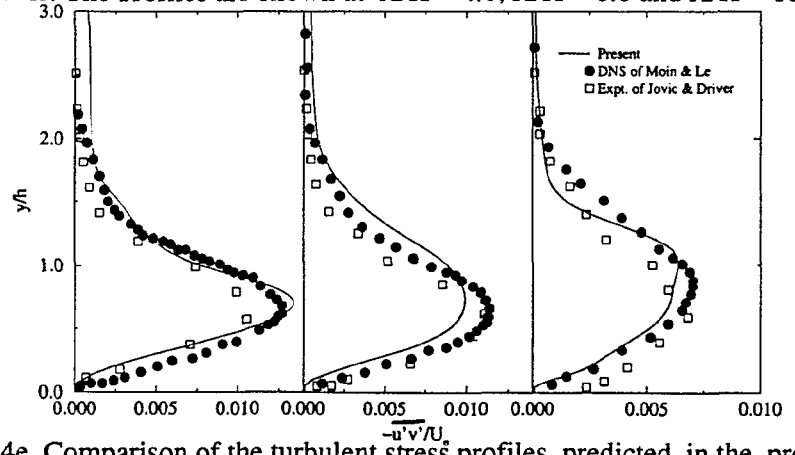

Fig. 4e. Comparison of the turbulent stress profiles predicted in the present simulations against DNS of Moin and Le and experiments of Jovic and Driver. The profiles are shown at X/H = 4.0, X/H = 6.0 and X/H = 10.0.

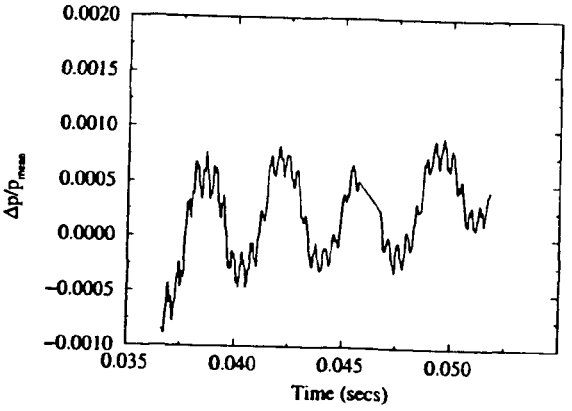

Fig. 5a. Pressure–Time trace in the combustor at X/h = 8.0 and Y/H = 1.2 for the dump combustor configuration without the area blockage lip at the exit.

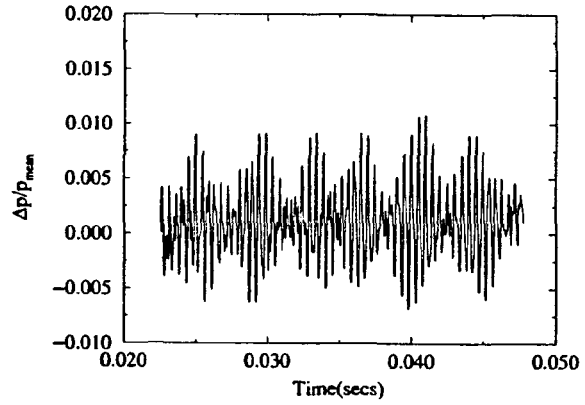

Fig. 5b. Pressure–Time trace in the combustor at X/h = 8.0 and Y/H = 1.2 for the dump combustor configuration with the area blockage lip at the exit.

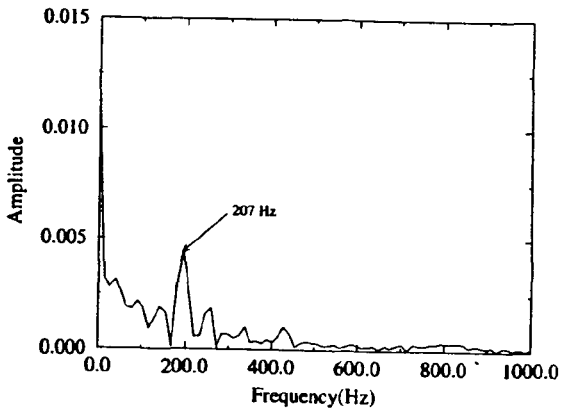

Fig. 5c. Fourier transform of the pressure–time trace shown in Fig.5a

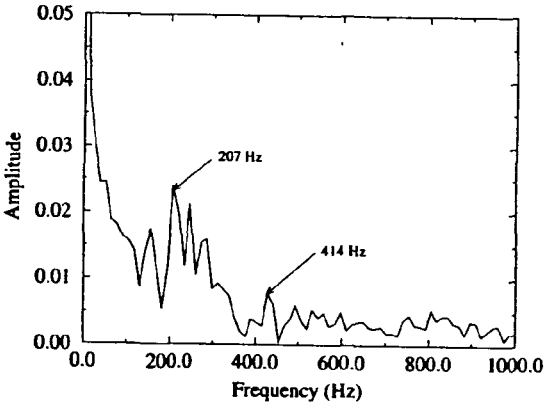

Fig. 5d. Fourier transform of the pressure–time trace shown in Fig.5b

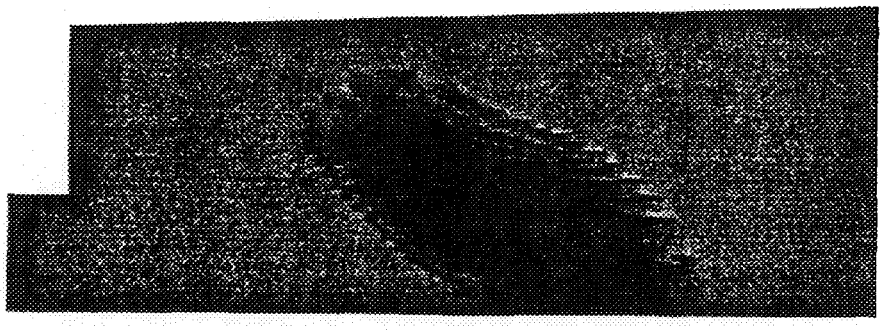

Fig. 6a. Hydroxyl radical concentration map for the unforced case. The snapshot is taken at time $tU_o/L = 100$.

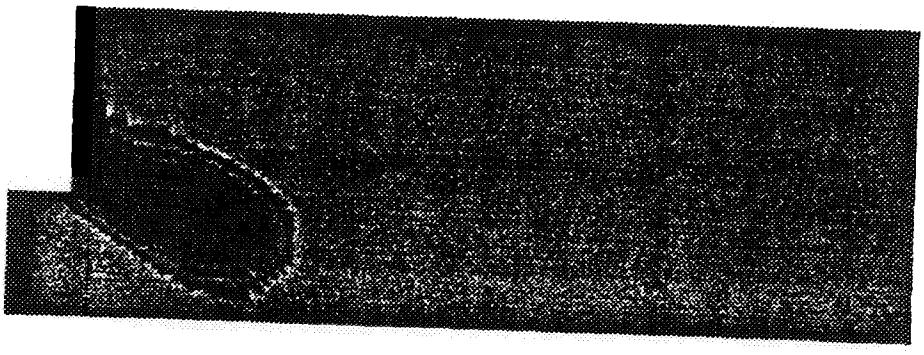

Fig. 6b. Hydroxyl radical concentration map for the inlet and fuel forced case. The snapshot is taken at time $tU_o/L = 100$.

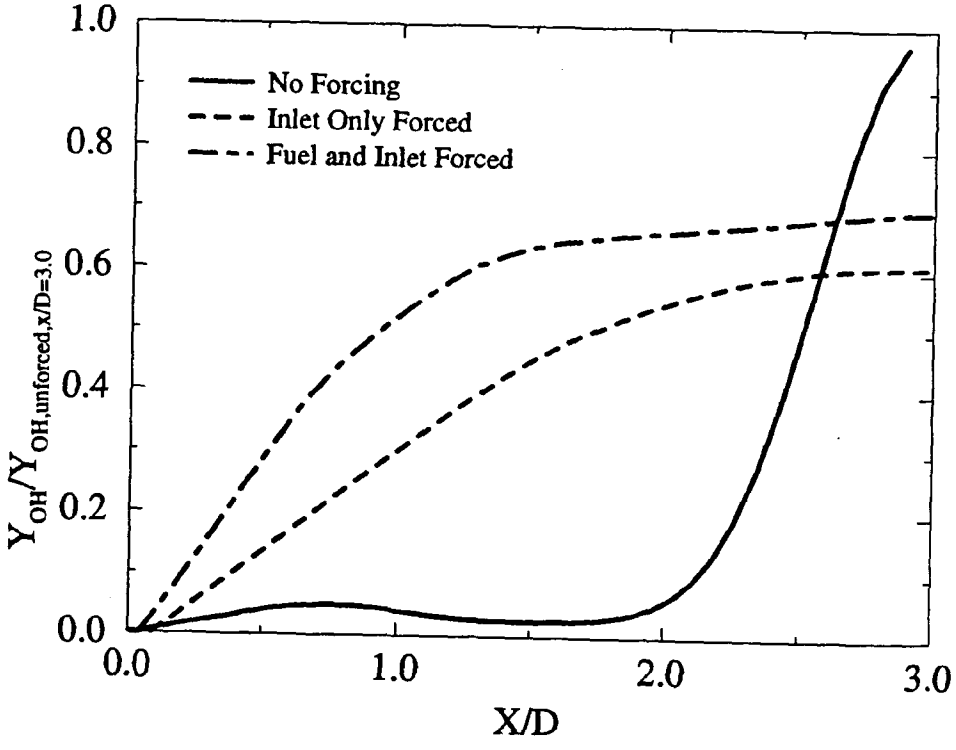

Fig. 7. Comparison of radially integrated mean Hydroxyl radical concentration profiles .

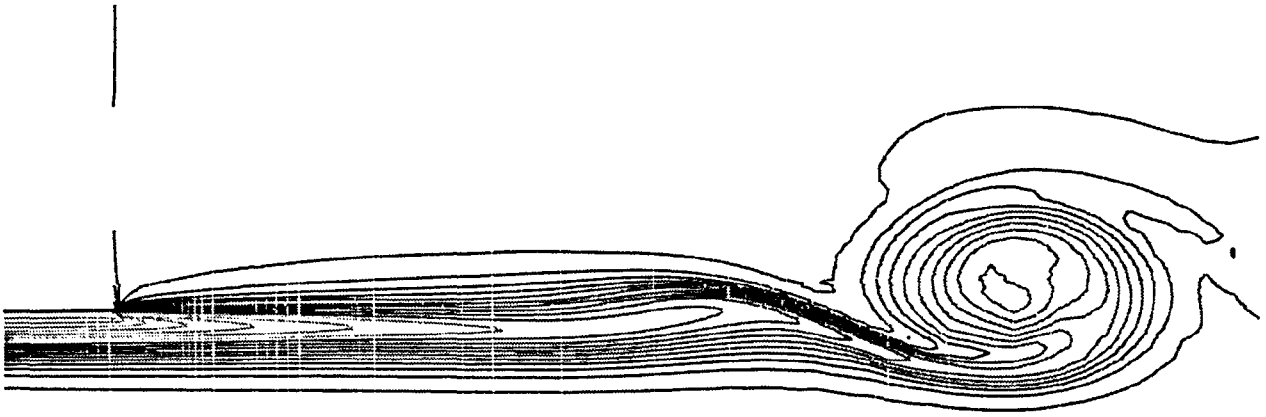

Fig. 8a. Vorticity Contours in the vicinity of the dump plane for the unforced case..

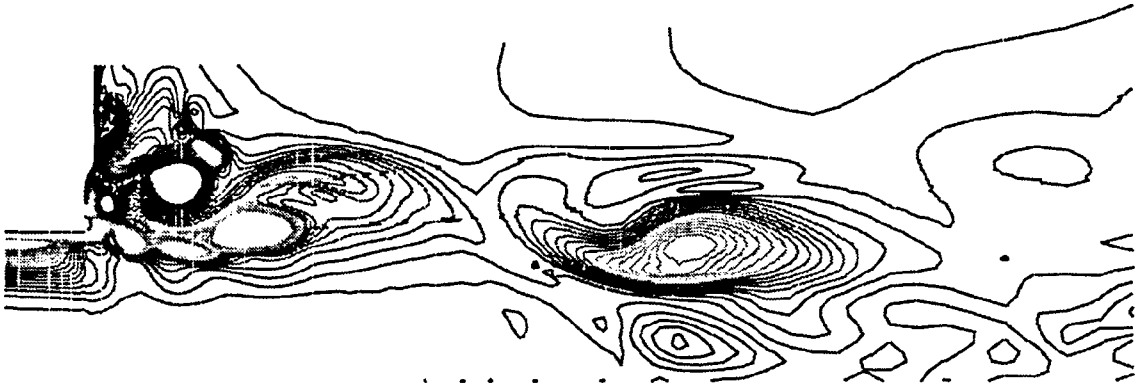

Fig. 8b. Vorticity Contours in the vicinity of the dump plane for the Inlet only forced case..

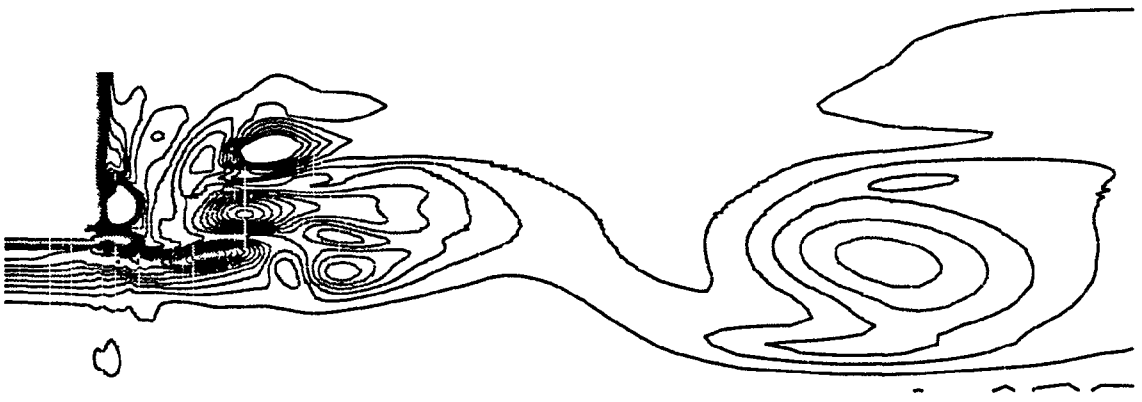

Fig. 8c. Vorticity Contours in the vicinity of the dump plane for the Inlet and Fuel forced case.

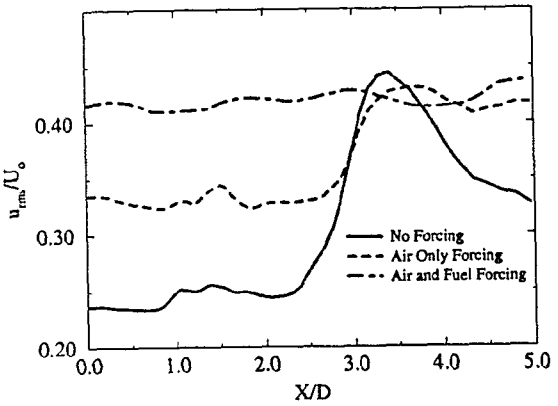

Fig. 9a. Comparison of the normalized turbulence intensity profiles along the shear layer center line for the forced and unforced cases.

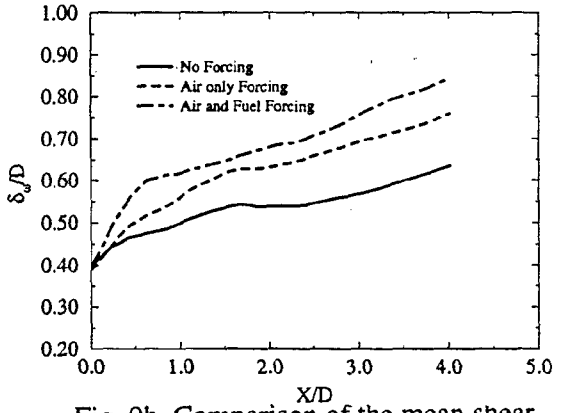

Fig. 9b. Comparison of the mean shear layer thickness for the forced and unforced cases.

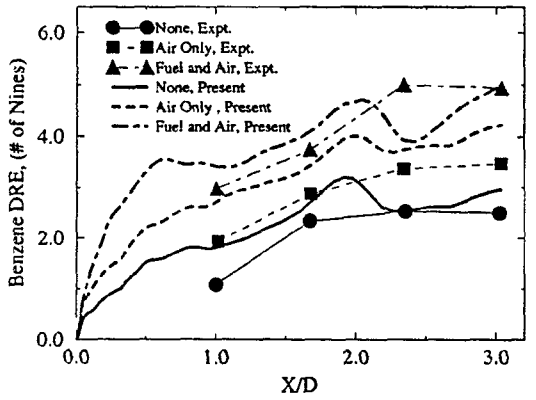

Fig. 10 Benzene consumption DRE's as a function of axial distance for the forced and unforced cases.